Research Square

Preprints are preliminary reports that have not undergone peer review.
They should not be considered conclusive, used to inform clinical practice,
or referenced by the media as validated information.

Estimating amyloid-β deposition using brain perfusion SPECT in Alzheimer's disease

Takashi Nakata

tnakata@hgmc.hyogo.jp

Hyogo Prefectural Harima-Himeji General Medical Center

Kenichi Shimada

Hyogo Prefectural Harima-Himeji General Medical Center

Haruhiko Oda

Hyogo Mental Health Center

Akira Terashima

Hyogo Prefectural Harima-Himeji General Medical Center

Yuko Suenaga

Hyogo Prefectural Harima-Himeji General Medical Center

Ryota Kawasaki

Hyogo Prefectural Harima-Himeji General Medical Center

Takahiro Yamada

Kindai University

Kazunari Ishii

Kobe University Graduate School of Medicine

Research Article

Keywords: Alzheimer's disease (AD), cerebrospinal fluid (CSF) biomarker, single photon emission computed tomography (SPECT), regional cerebral blood flow (rCBF), voxel-wise analysis, logistic regression analysis

Posted Date: August 19th, 2026

DOI: https://doi.org/10.21203/rs.3.rs-10624411/v1

License: This work is licensed under a Creative Commons Attribution 4.0 International License.
Read Full License

Additional Declarations: No competing interests reported.

Abstract

Purpose:

Alzheimer's disease (AD) involves amyloid-β (Aβ) and phosphorylated tau (p-tau) pathology. We aimed to investigate the correlation between the Aβ deposition and the regional cerebral blood flow (rCBF) using single photon emission computed tomography (SPECT) in AD suspected subjects.

Methods:

In this retrospective study, 88 patients underwent Mini-Mental State Examination (MMSE), MRI, perfusion SPECT, and cerebrospinal fluid (CSF) biomarker assessments. Voxel-wise analyses identified the regions where decreased rCBF correlated with CSF biomarkers. Logistic regression analysis was performed to examine the correlation between the presence or absence of Aβ deposition and each rCBF. Receiver operating characteristic (ROC) curve analysis was performed to evaluate diagnostic performance of each rCBF for Aβ deposition.

Results

Voxel-wise analysis revealed positive correlations between CSF Aβ42 and rCBF in posterior cingulate and angular gyrus, while CSF t-tau and p-tau181 correlated negatively with parietal hypoperfusion. CSF Aβ40 showed no significant correlation. Logistic regression analysis yielded the moderate correlation between Aβ deposition and left parietal rCBF compared with CSF biomarkers (Aβ42, p-tau181, t-tau, AD index and p-tau/Aβ42 ratio). ROC curve analysis revealed that the correlation between Aβ deposition and each rCBF tended to show lower AUC of approximately 0.7 compared to CSF biomarkers.

Conclusion

Brain perfusion SPECT revealed AD-typical hypoperfusion patterns and demonstrated modest potential to estimate the presence or absence of Aβ deposition with left parietal rCBF. Although perfusion SPECT cannot substitute CSF biomarker or amyloid/tau PET, perfusion SPECT may serve as a supportive triage tool to identify patients prior to amyloid PET.

Introduction

Alzheimer's disease (AD) [1, 2] is a progressive neurodegenerative disorder and the most common type of dementia around the world. AD is pathologically characterized by senile plaques and neurofibrillary tangles, the main components of which are amyloid-β (Aβ) and phosphorylated tau (p-tau), respectively [3, 4].

In recent years, monoclonal antibodies targeting Aβ have been approved, but their therapeutic effect is limited to the prodromal and early stages including the mild cognitive impairment (MCI) and the mild dementia phase [5–7]. The biological definition of AD pathology can be confirmed either by cerebrospinal fluid (CSF) biomarkers or amyloid positron emission tomography (PET) [8, 9], serving for cerebral Aβ deposition. Although amyloid PET demonstrates high diagnostic accuracy, the widespread clinical use of amyloid PET remains limited yet by cost and accessibility [10–12].

Amyloid positron emission tomography (PET) is less invasive but costly and usually limited to a single reimbursed scan [13–15], this examination is expensive and only single scanning under medical insurance coverage in Japan [14, 16]. 2-Deoxy-2-[^{18}F]-fluoro-D-glucose positron emission tomography (FDG-PET) has been extensively used in dementia research, however it does not directly reflect Aβ deposition; the clinical application is restricted; not covered by health insurance in most countries and the associated costs remain substantial. In contrast, single photon emission computed tomography (SPECT), which does not directly reflect Aβ deposition but provides information on regional cerebral blood flow (rCBF) patterns and reflects neuronal activity, has the advantage that is relatively inexpensive and can be used under health insurance coverage in dementia clinical practice [16–18]. Brain perfusion SPECT is particularly used for differentiating subtypes of neurodegenerative dementia in clinical practice [19], because characteristic hypoperfusion in the posterior cingulate cortex, precuneus, and temporoparietal regions has long been recognized in AD. However, this hypoperfusion can occur not only in AD but also in other neurodegenerative and cerebrovascular diseases [20].

The aim of this study was to evaluate the extent to which the presence or absence of Aβ deposition can be predicted using perfusion SPECT in a real-world clinical setting, prior to performing amyloid PET scans or CSF biomarker assessments. To investigate the confidence in the likelihood of AD, we evaluated the extent to which regional reductions in rCBF predict amyloid deposition and correlation between decreased rCBF and CSF biomarker levels.

Subjects and Methods

Subjects

We retrospectively selected the clinical and imaging data from the patients admitted to the infirmary at Hyogo Prefectural Harima-Himeji General Medical Center (formerly called Hyogo Brain and Heart Center) for the evaluation of dementia between January 2014 and March 2024.

During this period, 7,542 first-visit patients were screened. Of these, 245 patients met the following inclusion criteria: (i) age > 40 years; (ii) presence of clinical symptoms with MMSE score; (iii) availability of T1-weighted MRI and IMP-SPECT; (iv) availability of CSF biomarkers (CSF Aβ42, CSF Aβ40, CSF phosphorylated tau181 [p-tau], and CSF total tau [t-tau]). After excluding 157 patients with missing or confounding data (e.g., cerebrovascular disease, epilepsy, encephalitis, depression, and schizophrenia), 88 patients remained (Fig. 1). All 88 patients were examined by neurologists and psychiatrists and

underwent standard neurological and neuropsychological examinations, laboratory testing, head MRI, and brain perfusion SPECT (Table 1).

In this study, typical AD was defined as an amnestic-predominant clinical syndrome characterized by early and prominent episodic memory impairment, consistent with the classical hippocampal-type AD. All typical AD met the diagnostic criteria for probable AD according to the National Institute on Aging–Alzheimer's Association (NIA–AA) guidelines, and did not exhibit clinical features of atypical AD variants, such as posterior cortical atrophy, logopenic variant primary progressive aphasia, or frontal variant AD [8, 9, 21–25].

Clinical symptoms included fluctuation in cognitive function, recurrent visual hallucinations, auditory hallucinations, spontaneous parkinsonism, rapid eye movement sleep behavior disorder (RBD), visual/visuospatial cognitive impairment, gait disturbance, hearing loss, urinary disturbance, attention dysfunction, apraxia, insomnia, depression, delusion, irritation and agitation.

CSF Biomarker Measurement

All of CSF samples were outsourced for testing over a period of 10 years. CSF samples were collected by lumbar puncture, stored at -80℃, and analyzed using two assay platforms: Infinite® F50R (enzyme immunoassay [EIA]; FUJIFILM Wako Pure Chemical Corporation, Osaka, Japan) [26, 27] and LUMIPULSE® G1200 (chemiluminescent enzyme immunoassay [CLEIA]; FUJIREBIO Inc., Tokyo, Japan) [28, 29]. CSF Aβ42, CSF Aβ40, CSF t-tau and CSF p-tau levels were measured, while patient's information and clinical data were blinded. In our study, CSF AD Index was calculated on CSF t-tau × CSF Aβ40/Aβ42 [30, 31].

Brain Perfusion SPECT and MRI Acquisition

Details of the brain perfusion SPECT procedure are provided elsewhere [17, 18]. In brief, brain perfusion SPECT scans were initiated in the resting state with the eyes closed, 15 minutes after each patient was administered an injection of 111 MBq of *N*-isopropyl-*p*-[^{123}I]-iodoamphetamine. All SPECT scans were performed using a rotating dual-headed gamma camera (E-CAM, Siemens, Erlangen, Germany) with a low–medium energy, general purpose collimator. Brain perfusion SPECT images were obtained with a 128 × 128 matrix, 2.5 minutes/rotation × 12 rotations. For SPECT image reconstruction, a Butterworth filter (cutoff frequency: 0.58 cycles/cm, order: 8) was used. Attenuation correction was performed using Chang's method ($\mu = 0.09\ cm^{-1}$) and scatter correction was performed with a triple energy window.

MRI scanning was performed using a 3 T Achieva or a 1.5 T Ingenia (Philips, Best, Netherlands). The scan protocol included sagittal T1-weighted three-dimensional whole-brain images (Achieva: slice thickness 1.2 mm, 140 slices, matrix size 256 × 256, field of view 25.6 × 25.6 cm, echo time 3.11 ms, repetition time 6.7 ms, flip angle 8°; Ingenia: slice thickness 1.2 mm, 140 slices, matrix size 192 × 192, field of view 24.0 × 24.0 cm, echo time 4.0 ms, repetition time 8.6 ms, flip angle 8°). A 3 T Achieva or 1.5

T Ingenia scanner was performed under each condition, total scan duration time 3 min 30 s or 3 min 47 s, and acceleration factor 2 each other. To obtain rCBF values, the voxel counts for each SPECT image were normalized by dividing them by the cerebellar count [10, 17, 18, 32] measured with our homemade cerebellar voxels of interest (VOIs), because global cerebral blood flow is often decreased in AD and normalization according to the global counts may lead to underestimation of rCBF values [33].

Data Analysis

In the following three steps, the aims of this study were to: (i) identify regions of rCBF reduction common to AD, (ii) examine correlations between the presence or absence of Aβ deposition and rCBFs of AD specific regions, MMSE, age, and sex by logistic regression analysis, and (iii) evaluate the diagnostic performance of the generalized linear models obtained by stepwise linear regression analysis.

Voxel-wise analysis was performed using Statistical Parametric Mapping 12 (SPM12) (https://www.fil.ion.ucl.ac.uk/spm/software/spm12/). The correlation between decreased rCBF in SPECT and CSF biomarker levels was evaluated.

SPECT data were normalized to cerebellar counts and each individual SPECT image was co-registered to the corresponding MRI. The MRI was segmented into gray matter (GM), white matter, and CSF using the SPM12 segmentation program. GM images were spatially normalized to a standard template using Diffeomorphic Anatomical Registration Through Exponentiated Lie Algebra (DARTEL) [34]. The resulting normalization parameters were applied to the co-registered SPECT images, which were then spatially normalized to the Montreal Neurological Institute (MNI) space. All images were smoothed with a 12 mm Gaussian filter. Next, SPM12 was used for voxel. Voxel-wise analysis was performed between GM or CBF images and CSF biomarker levels, MMSE scores, age or sex. The significance threshold was set at $p < 0.001$ (uncorrected), with a voxel extent threshold of 300.

First, we defined the regions of significantly reduced rCBF common in AD patients.

Next, the normality of each dataset was assessed using normal Quantile-Quantile plot (Q-Q plot).

Third, we investigated whether the presence or absence of Aβ deposition could be estimated based on rCBF of three VOIs (the posterior cingulate [PC] and bilateral parietal regions [Par]) in SPECT imaging. Receiver operating characteristic (ROC) curve analysis was performed to evaluate diagnostic performance of each rCBF for Aβ deposition compared with CSF biomarkers.

Further, univariate logistic regression analysis was performed using CSF Aβ42/40 ratio as an indicator of Aβ deposition based on a cut off value of 0.067 mg/dl [29]; below 0.067 mg/dl as positive and with 0.067 mg/dl or higher were classified as negative. Correlation between CSF Aβ42/40 ratio and each rCBF of three VOIs was compared with CSF biomarkers, MMSE scores, age, and interval days between MRI and SPECT examinations.

Moreover, we evaluated a model equation incorporating each rCBF of the three VOIs, MMSE scores, age, sex, and interval days between MRI and IMP-SPECT using multivariate logistic regression analysis. The final model for predicting the presence or absence of Aβ deposition was constructed and optimized by stepwise linear regression analysis based on the Akaike's Information Criterion (AIC).

Results

Patient Characteristics

The final cohort comprised 88 patients (31 males, 57 females; mean age 70.5 ± 10.9 years [range: 43–87 years]; mean MMSE score 23.2 ± 4.9 [rage: 8–30]). Among them, 35 patients exhibited underlying AD pathology, including typical AD (described above in detail), mild cognitive impairment (MCI) due to AD, posterior cortical atrophy (PCA)-AD, corticobasal syndrome (CBS)-AD, and AD with comorbid idiopathic normal pressure hydrocephalus (iNPH). The remaining 53 patients had non-AD diagnoses such as dementia with Lewy bodies (DLB), classified according to the established diagnostic criteria. Table 1 summarizes patient characteristics. The mean age was 71.5 years in males and 68.2 years in females. The mean MMSE score was 23.2 points for males and 22.6 points for females; AD group (n = 35): mean age 69.5 ± 11.4 years (range: 49–86 years), mean MMSE score 22.8 ± 4.7 points (range: 14–30 points); non-AD group (n = 53): mean age 71.2 ± 10.7 years (range: 43–87 years), mean MMSE score 23.4 ± 5.1 points (range: 8–30 points).

Clinical Symptoms

Table 2 presents the clinical symptoms and neuropsychological findings. Parkinsonism and visual/visuospatial cognitive impairment were observed in both AD and non-AD groups. However, gait disturbance was significantly more frequent in non-AD patients ($p = 0.010$, Student's t-test).

Voxel-wise Analysis of CSF Biomarkers and Brain Perfusion SPECT

The correlations between rCBF from SPECT and CSF biomarker levels are summarized in Table 3 and Fig. 2. In the AD group: CSF Aβ42 level was positively correlated with rCBF in the right ventral posterior cingulate (Brodmann area [BA] 23), left angular gyrus (BA39), and right medial temporal gyrus (BA21). CSF Aβ40 and sex presented no significant correlations. The Aβ42/40 ratio showed positive correlations in bilateral angular gyri. In contrast, the CSF AD Index [30, 31], CSF t-tau, and p-tau levels were negatively correlated with the angular gyrus. MMSE scores were positively correlated with the inferior and medial temporal gyri, posterior cingulate, and frontal eye fields, and negatively correlated with premotor regions. Age correlated positively with the somatosensory and visual association cortices, and negatively correlated with the insula, posterior cingulate, and parahippocampal gyrus.

Assessment of Data Normality

An assessment of data normality using normal Q-Q plot revealed that, with the exception of interval days between MRI and IMP-SPECT, the data exhibited an approximately normal distribution within an acceptable range (Fig. 3). Regarding the CSF p-tau/Aβ42 ratio, Aβ42, Aβ40, p-tau, t-tau, and interval days, the graphs showed a tendency toward slight positive skewness; the deviation toward the upper right was particularly pronounced for interval days.

Correlation between CSF Aβ42/40 ratio and rCBF of each VOI

Figure 4 compares the correlations of the CSF Aβ42/40 ratio with the rCBF of each VOI, individual CSF biomarkers, MMSE score, age, and interval days. Correlation strength and statistical significance were evaluated using Pearson's correlation coefficients (PCCs; *r*) and corresponding p values. The correlations between the rCBF of each VOI and the CSF Aβ42/40 ratio, as an indicator of Aβ deposition, showed lower PCCs than those between individual CSF biomarkers (e.g., p-tau/Aβ42 ratio, AD index, p-tau, and t-tau) and the CSF Aβ42/40 ratio. In contrast, the correlations of MMSE score, age, and interval days with the CSF Aβ42/40 ratio were weaker than those between the rCBF of each VOI and the CSF Aβ42/40 ratio.

Receiver Operating Characteristic (ROC) Curve Analysis

Figure 5 showed the assessment of Aβ deposition status in 88 patients, based on each rCBF of three VOIs, with the CSF Aβ42/40 ratio serving as the criterion for the presence or absence of Aβ deposition; Aβ deposition positivity was defined cutoff 0.067 mg/dl [29] as CSF Aβ42/40 ratio of less than 0.067 mg/dl and negativity as 0.067 mg/dl or higher. Estimation of Aβ deposition based on each rCBF of VOI tended to show lower area under the curve (AUC) compared to CSF biomarkers (approximately 0.7). Correlations with Aβ deposition were even weaker than each rCBF for MMSE scores, age, and the interval days between MRI and SPECT examinations.

Univariate Logistic Regression Analysis and Model Equation using each rCBF of VOI

In 88 patients, the CSF Aβ42/40 ratio was set as the criterion for Aβ deposition; univariate logistic regression analysis was performed to examine the correlation between the rCBF value of each VOI and the presence or absence of Aβ deposition, with the results presented in Table 4. Each rCBF of three VOIs, CSF biomarker concentration, MMSE score, age, and interval days were selected as variables; the model was expressed as a linear equation, and statistical significance was evaluated. The correlation between CSF Aβ42/40 ratio and each rCBF of VOI was shown in Fig. 5, PCC was calculated. Comparisons were made with each CSF biomarker level, MMSE score, age, and interval days between imaging examinations.

Multivariate Logistic Regression Analysis and Generalized Linear Model by Stepwise Linear Regression Analysis

In 88 patients, multivariate logistic regression analysis was performed using the presence or absence of Aβ deposition—defined based on the CSF Aβ42/40 ratio—as the dependent variable and following factors (e.g., each rCBF of VOI, MMSE score, age, sex, and interval days) as independent variables; the results are presented in Table 5. Furthermore, the generalized linear model was determined by stepwise linear regression analysis based on the Akaike's Information Criterion (AIC). The final model was obtained as Aβ deposition ≈ − 6.353 × rCBF_ltPar + 3.955 (odds ratio: 1.74×10^{-3}; 95% confidence interval [CI]: 2.58×10^{-5}, 1.18×10^{-1}; p-value: 3.12×10^{-3}), as shown in Table 6. The variance inflation factor (VIF) was in the range of 2–4.

Discussion

This study identified AD-typical hypoperfusion in the parietotemporal and PC regions, consistent with findings reported in previous FDG-PET studies [35]. Correlations between rCBF derived from brain perfusion SPECT and CSF biomarkers were modest but directionally concordant with earlier reports [36–41].

First, voxel-wise analyses revealed that CSF Aβ42 levels were positively correlated with rCBF in PC, the angular gyrus, and medial temporal cortex (Fig. 2 and Table 3). Similarly, the CSF Aβ42/40 ratio correlated positively with the angular gyrus, while CSF t-tau and CSF p-tau were negatively correlated within overlapping cortical areas. MMSE score was positively correlated with hypoperfusion in the temporal and cingulate cortices, and negatively correlated with the premotor cortex. Age exhibited both positive and negative correlations across multiple brain regions. These findings are consistent with previous FDG-PET studies reporting the parietotemporal and PC hypometabolism in AD [35], providing complementary insights into the CSF biomarker level–rCBF correlations.

As shown in Fig. 3, Q-Q plots indicated that, with the exception of interval days, the data fell within an acceptable range and approximated a normal distribution. In this study, the dataset was determined to satisfy the assumption of normality. We examined the correlations between the presence or absence of Aβ deposition and various parameters, including rCBF, CSF biomarkers, MMSE, age, and interval days.

In Fig. 4, while PCC between Aβ deposition and rCBF was statistically significant ($p < 0.05$), the r was approximately 0.38, indicating a weak correlation compared to CSF biomarkers. We believe that it is difficult to replace CSF biomarkers with rCBF for predicting the presence or absence of Aβ deposition.

Figure 5 demonstrated that left parietal rCBF yielded an AUC of 0.72, representing the best performance among the three VOIs; the others showed AUC below 0.7. Each AUC for MMSE, age, and interval days was low, ranging from approximately 0.4 to 0.6. Meanwhile, the CSF AD Index demonstrated the best performance with an AUC of 0.90; however, even CSF p-tau—a marker expected to show high diagnostic accuracy—yielded an AUC of 0.79, falling short of the 0.9 and higher value we had initially anticipated. Nevertheless, while an AUC of 0.72 for left parietal rCBF is not particularly high, the fact that CSF p-tau also showed an AUC below 0.8 suggests that the left parietal rCBF might not be considered statistically

low. Furthermore, we evaluated using logistic regression analysis whether the presence or absence of Aβ deposition could be directly inferred from rCBF.

Table 3 indicates that the CSF AD Index, p-tau, t-tau, and Aβ42 showed statistically significant correlations with the presence or absence of Aβ deposition. The left parietal rCBF among the VOIs was the most significant (almost without laterality), though its performance was slightly inferior to that of the aforementioned CSF biomarkers. Previous studies have demonstrated that CSF Aβ positivity is strongly associated with cortical Aβ deposition in regions comprising the default mode network (DMN), including the posterior cingulate cortex (PCC), precuneus, medial frontal cortex, and lateral parietal association cortex [42]. Furthermore, in typical Alzheimer's disease (AD), no hemispheric asymmetry in the distribution of Aβ deposition has been observed on amyloid PET and structural MRI [43]. These our findings were in line with previous studies reporting the characteristic distribution pattern of Aβ deposition in typical AD.

The univariate logistic regression analysis revealed that the statistical significance of the correlation between rCBF in each VOI and the presence or absence of Aβ deposition was lower than that of the correlation between CSF biomarkers and the presence or absence of Aβ deposition—even for the left parietal rCBF where the correlation was strongest among three VOIs (Table 4).

Table 5 presents the results of a multivariate logistic analysis regarding the correlation between the presence or absence of Aβ deposition and seven parameters. In this model, the model incorporating all seven independent variables factors was not statistically significant. Subsequently, the multivariate model using these seven variables was statistically optimized into a final model by a stepwise method based on AIC. As shown in Table 6, the final model was expressed as a very simple linear equation with left parietal rCBF as the sole factor and was statistically significant. These findings suggest that a linear model equation using the left parietal rCBF value—specifically focusing on the left parietal VOI—as a factor could serve as a potential tool for providing supplementary diagnostic information regarding the presence or absence of Aβ deposition.

Recent studies have shifted SPECT analysis from qualitative assessment toward quantitative imaging biomarker modeling, a few pioneering studies have been reported. In a previous study, [^{99m}Tc]-ECD-SPECT conducted to predict Aβ positivity using easy Z-score imaging system (eZIS) [36]. The presence or absence of Aβ deposition was evaluated using a generalized additive model (GAM) that integrated three indices (severity, extent and ratio) derived from cerebral blood flow SPECT with MMSE scores, age, and sex. Amyloid PET served as the reference standard for Aβ deposition status; the best performance achieved was an AUC of 0.818 [36].

Recently, the prediction of Aβ PET positivity based on a combination of MRI and SPECT was reported [44]. MRI analysis using voxel-based specific regional analysis system for atrophy detection yielded an AUC of 0.72. Visual assessment combining MRI and cerebral blood flow SPECT resulted in an AUC of 0.767, showing no statistically significant improvement compared to MRI alone [44]. This finding indicates that while VSRAD analysis of MRI data demonstrated moderate statistical significance, SPM

and voxel-based assessment of MRI and SPECT combination did not observe significant difference. Even the most promising modality (MRI and SPECT) combination had an AUC of around 0.77 with visual assessment [44], which is almost the same level as our results in SPM/DARTEL method and voxel-wise analysis, and their MRI and SPECT combination clearly did not yield a significantly high diagnostic performance.

Woyk K, et al. reported that FDG-PET uptake was positively correlated with CSF Aβ42 in PC (r = 0.38) and parietal cortex (r = 0.39), and parietal uptakes were associated with CSF Aβ42/40 ratio (r = 0.34). Conversely, uptakes in prefrontal cortex (r = − 0.41), PC (r = − 0.24), and parietal cortex (r = − 0.28) were negatively correlated with CSF t-tau, while prefrontal (r = − 0.36) and parietal cortex (r = − 0.27) uptakes were negatively correlated with CSF p-tau [37]. Similar patterns were observed with FDG uptake across the frontal, PC, parietal, and temporal cortices, indicating positive correlations with CSF Aβ42 (r = 0.28–0.35) and negative correlations with CSF t-tau (r = − 0.36 to − 0.22) and CSF p-tau (r = − 0.31 to − 0.18) [45]. Previous investigations closely aligned with our results. Brain perfusion SPECT and FDG-PET have indicated significant correlations with CSF biomarkers, however r values were not as high as expected [37–40, 45]. Discrepancies involving CSF Aβ40 may reflect methodological differences or cohort characteristics.

In contrast, arterial spin labelling (ASL) MRI has shown potential to have diagnostic capabilities similar to FDG-PET, with particularly high reproducibility of reduced cerebral blood flow in the hippocampus, precuneus and posterior cingulate regions; the combination of ASL and structural MRI is expected to be promising [46].

Recent imaging-based predictive approaches have focused on amyloid PET [13, 34–37, 45]. While methods such as the easy Z-score imaging system (eZIS) and specific VOI analysis (SVA) predict amyloid PET positivity [36], this study differs by applying SPM12/DARTEL-based voxel-wise analysis [34] and directly predicting numerical CSF biomarker concentrations using multiple regression models. Advanced machine-learning approaches using FDG-PET, including support vector machine models, have reported high predictive accuracy for amyloid PET status [13].

Further, recent advances suggest that artificial intelligence and machine-learning approaches may enhance the predictive value of multimodal neuroimaging [47]. In future, implementation of more advanced artificial intelligence (AI) models may improve predictive accuracy and clinical usability. Our research group plans to report these results elsewhere.

These findings highlight the potential of this approach that brain perfusion SPECT may reflect not only neurodegeneration caused by Aβ deposition but also the influence of cerebral blood flow and that brain perfusion SPECT–based prediction of Aβ deposition as a supportive triage tool prior to amyloid PET may serve as a practical adjunct for early diagnosis, clinical decision-making and reducing caregiver burden. We believe that PET is expensive and available at limited facilities despite its high accuracy, brain perfusion SPECT is considered useful due to more cost-effectiveness and greater accessibility than FDG-PET or amyloid-PET. To improve the prediction performance, further improvements are expected through

the use of more advanced artificial intelligence models, the conduct of large prospective studies and the combination with neuroimaging modalities.

Limitations

This study has several limitations. First, it was retrospective with a relatively small sample of 88 cases. Second, the data were collected before the approval of anti-Aβ monoclonal antibodies [5], and included several atypical AD variants [21, 22], complicating interpretation. Third, the CSF biomarker assays were performed at different laboratories using varying platforms across the 10-year period, introducing potential variability. Moreover, Japanese health insurance coverage allows only a single amyloid PET or CSF test for Aβ pathology per a patient, limiting simultaneous CSF biomarker validation. Research budgetary constraints also precluded concurrent PET and CSF evaluations. In the ATN framework, brain perfusion SPECT primarily reflects the neurodegeneration (N) marker, which may partly explain the weak correlations with amyloid (A) and tau (T) marker [48]. Without concurrent amyloid or tau PET [49], the correlation between SPECT rCBFs and Aβ deposition remains modest as similar to FDG-PET.

Conclusion

In summary, brain perfusion SPECT revealed AD-typical perfusion patterns, the presence or absence of Aβ deposition correlated moderately with particularly the left parietal rCBF in SPECT imaging. Although SPECT cannot completely substitute amyloid/tau PET or CSF biomarker measurements, brain perfusion SPECT may serve as a supportive tool for triaging patients prior to amyloid PET. Further studies are needed to improve the predictive potential of Aβ deposition derived from brain perfusion SPECT in AD.

Abbreviations

AD, Alzheimer's disease; Aβ, amyloid-β; p-tau; phosphorylated tau; MCI, mild cognitive impairment; CSF, cerebrospinal fluid; PET, positron emission tomography; [^{18}F]-FDG, 2-deoxy-2-[^{18}F]-fluoro-D-glucose; SPECT, single photon emission computed tomography; rCBF, regional cerebral blood flow; SUVR, the standardized uptake value ratio; VOI, voxel of interest; MMSE, Mini-Mental State Examination; MRI, magnetic resonance imaging; NIA–AA, the National Institute on Aging–Alzheimer's Association; RBD, rapid eye movement sleep behavior disorder; EIA, enzyme immunoassay; CLEIA, chemiluminescent enzyme immunoassay; [^{123}I]-IMP, *N*-isopropyl-*p*-[^{123}I]-iodoamphetamine; SPM12, Statical Parametric Mapping 12 Software; GM, gray matter; DARTEL, Diffeomorphic Anatomical Registration Through Exponentiated Lie Algebra; MNI space, Montreal Neurological Institute space; Q-Q plot, Quantile-Quantile plot; PC, posterior cingulate; Par, parietal cortex; AIC, Akaike's Information Criterion; PCA, posterior cortical atrophy, CBS, corticobasal syndrome; iNPH, idiopathic normal pressure hydrocephalus; DLB, dementia with Lewy bodies; BA, Brodmann area; ROC curve analysis, receiver operating characteristic curve analysis; AUC, area under the curve; PCC, Pearson's correlation coefficient; VIF, variance inflation factor; DMN, default mode network; [^{99m}Tc]-ECD, [^{99m}Tc]-Technetium-99-ethyl cysteinate dimer; eZIS,

easy Z-score imaging system; ASL, arterial spin labelling; AI, artificial intelligence; ATN, amyloid-tau-neurodegeneration

Declarations

Ethics Approval: This study was approved by the ethics committee of the hospital with which the corresponding author is affiliated. The requirement for written informed consent was waived due to the retrospective nature of the study. Informed Consent: All investigations were carried out according to the Declaration of Helsinki. We confirmed that we have read the Journal's position on issues involved in ethical publication and affirm that this report is consistent with those guidelines. All co-authors have read and approved the submission. This study was examined by the ethics committee of the corresponding author's affiliated hospital, and informed consent was made by opt-out information disclosure.

Author Contribution

Conceptual idea for the article was by TN and KI. TN performed the literature search. TN, KS, HO, and AT were involved in the clinical neurological and neuropsychological data acquisition. YS, RK, and KI were involved in the imaging data acquisition. TN, TY and KI performed the data analysis. The first draft of the manuscript was written by TN and was reviewed by KI. All authors provided critical revisions on previous versions of the manuscript. All authors read and approved the final manuscript.

Acknowledgement

We would like to express our gratitude to all hospital staff at the Hyogo Prefectural Harima-Himeji General Medical Center (formerly called Hyogo Brain and Heart Center) for providing us with the chance to perform this research. Special thanks to all patient and staff in the memory clinic in the Neurocognitive Disorders Medical Center at the Hyogo Prefectural Harima-Himeji General Medical Center.

Data Availability

The datasets used and/or analyzed during the current study are available from the corresponding author on reasonable request.

References

1. McKhann G, Drachman D, Folstein M, Katzman R, Price D, Stadlan EM (1984) Clinical diagnosis of Alzheimer's disease: report of the NINCDS-ADRDA Work Group under the auspices of Department of Health and Human Services Task Force on Alzheimer's Disease. Neurology 34(7):939–944
2. McKhann GM, Knopman DS, Chertkow H, Hyman BT, Jack CR Jr., Kawas CH et al (2011) The diagnosis of dementia due to Alzheimer's disease: recommendations from the National Institute on Aging-Alzheimer's Association workgroups on diagnostic guidelines for Alzheimer's disease. Alzheimers Dement 7(3):263–269
3. Hardy J, Selkoe DJ (2002) The amyloid hypothesis of Alzheimer's disease: progress and problems on the road to therapeutics. Science 297(5580):353–356
4. Braak H, Braak E (1991) Neuropathological stageing of Alzheimer-related changes. Acta Neuropathol 82(4):239–259
5. Yadollahikhales G, Rojas JC (2023) Anti-Amyloid Immunotherapies for Alzheimer's Disease: A 2023 Clinical Update. Neurotherapeutics 20(4):914–931
6. van Dyck CH, Swanson CJ, Aisen P, Bateman RJ, Chen C, Gee M et al (2023) Lecanemab in Early Alzheimer's Disease. N Engl J Med 388(1):9–21
7. Sims JR, Zimmer JA, Evans CD, Lu M, Ardayfio P, Sparks J et al (2023) Donanemab in Early Symptomatic Alzheimer Disease: The TRAILBLAZER-ALZ 2 Randomized Clinical Trial. JAMA 330(6):512–527
8. Jack CR Jr., Andrews JS, Beach TG, Buracchio T, Dunn B, Graf A et al (2024) Revised criteria for diagnosis and staging of Alzheimer's disease: Alzheimer's Association Workgroup. Alzheimers Dement 20(8):5143–5169
9. Jack CR Jr., Bennett DA, Blennow K, Carrillo MC, Dunn B, Haeberlein SB et al (2018) NIA-AA Research Framework: Toward a biological definition of Alzheimer's disease. Alzheimers Dement 14(4):535–562
10. Pemberton HG, Collij LE, Heeman F, Bollack A, Shekari M, Salvadó G et al (2022) Quantification of amyloid PET for future clinical use: a state-of-the-art review. Eur J Nucl Med Mol Imaging 49(10):3508–3528
11. Morris E, Chalkidou A, Hammers A, Peacock J, Summers J, Keevil S (2016) Diagnostic accuracy of (18)F amyloid PET tracers for the diagnosis of Alzheimer's disease: a systematic review and meta-analysis. Eur J Nucl Med Mol Imaging 43(2):374–385
12. Nordberg A, Rinne JO, Kadir A, Långström B (2010) The use of PET in Alzheimer disease. Nat Rev Neurol 6(2):78–87
13. Yamada T, Kimura Y, Watanabe S, Watanabe A, Honda M, Nagaoka T et al (2025) Evaluation of amyloid PET positivity using machine learning on (18)F-FDG PET images. Jpn J Radiol 43(9):1541–1549
14. Ruan D, Sun L (2023) Amyloid-beta PET in Alzheimer's disease: A systematic review and Bayesian meta-analysis. Brain Behav 13(1):e2850

15. Fantoni ER, Chalkidou A, JT OB, Farrar G, Hammers A (2018) A Systematic Review and Aggregated Analysis on the Impact of Amyloid PET Brain Imaging on the Diagnosis, Diagnostic Confidence, and Management of Patients being Evaluated for Alzheimer's Disease. J Alzheimers Dis 63(2):783–796
16. Ferrando R, Damian A (2021) Brain SPECT as a Biomarker of Neurodegeneration in Dementia in the Era of Molecular Imaging: Still a Valid Option? Front Neurol 12:629442
17. Nakata T, Shimada K, Iba A, Oda H, Terashima A, Koide Y et al (2024) Differential diagnosis of MCI with Lewy bodies and MCI due to Alzheimer's disease by visual assessment of occipital hypoperfusion on SPECT images. Jpn J Radiol 42(3):308–318
18. Nakata T, Shimada K, Iba A, Oda H, Terashima A, Koide Y et al (2022) Correlation between noise pareidolia test scores for visual hallucinations and regional cerebral blood flow in dementia with Lewy bodies. Ann Nucl Med 36(4):384–392
19. Matsuda H (2007) Role of neuroimaging in Alzheimer's disease, with emphasis on brain perfusion SPECT. J Nucl Med 48(8):1289–1300
20. Weih M, Degirmenci U, Kreil S, Lewczuk P, Schmidt D, Kornhuber J et al (2010) Perfusion Imaging with SPECT in the Era of Pathophysiology-Based Biomarkers for Alzheimer's Disease. Int J Alzheimers Dis 2010:109618
21. Dubois B, von Arnim CAF, Burnie N, Bozeat S, Cummings J (2023) Biomarkers in Alzheimer's disease: role in early and differential diagnosis and recognition of atypical variants. Alzheimers Res Ther 15(1):175
22. Graff-Radford J, Yong KXX, Apostolova LG, Bouwman FH, Carrillo M, Dickerson BC et al (2021) New insights into atypical Alzheimer's disease in the era of biomarkers. Lancet Neurol 20(3):222–234
23. Jack CR Jr., Bennett DA, Blennow K, Carrillo MC, Feldman HH, Frisoni GB et al (2016) A/T/N: An unbiased descriptive classification scheme for Alzheimer disease biomarkers. Neurology 87(5):539–547
24. Ossenkoppele R, Jansen WJ, Rabinovici GD, Knol DL, van der Flier WM, van Berckel BN et al (2015) Prevalence of amyloid PET positivity in dementia syndromes: a meta-analysis. JAMA 313(19):1939–1949
25. Dubois B, Feldman HH, Jacova C, Hampel H, Molinuevo JL, Blennow K et al (2014) Advancing research diagnostic criteria for Alzheimer's disease: the IWG-2 criteria. Lancet Neurol 13(6):614–629
26. Yamakami K, Matsubara T, Fujita K, Nakamura K, Kihara N, Sogawa K et al (2025) Identification of Hasegawa Dementia Scale-Revised Cutoff Scores Associated With Mini-Mental State Examination Thresholds for Anti-Amyloid β Therapies in Patients With Amnesia. Psychogeriatrics 25(6):e70107
27. Ozaki T, Hashimoto N, Narita H, Udo N, Mito S, Nakagawa S et al (2025) Association between higher cerebrospinal fluid levels of phosphorylated tau and reduced depressive symptoms in patients with cognitive decline. PCN Rep 4(4):e70228
28. Kurihara M, Kondo S, Ohse K, Nojima H, Kikkawa-Saito E, Iwata A (2024) Relationship Between Cerebrospinal Fluid Alzheimer's Disease Biomarker Values Measured via Lumipulse Assays and

Conventional ELISA: Single-Center Experience and Systematic Review. J Alzheimers Dis 99(3):1077–1092

29. Hisashi Nojima S, Ito A, Kushida A, Abe W, Motsuchi D, Verbel et al (2022) Clinical utility of cerebrospinal fluid biomarkers measured by LUMIPULSE system. Ann Clin Transl Neurol 9(12):1898–1909
30. Shoji M, Kanai M (2001) Cerebrospinal fluid Aβ40 and Aβ42: Natural course and clinical usefulness. J Alzheimers Dis 3(3):313–321
31. Shoji M (2002) CEREBROSPINAL FLUID Aβ40 AND Aβ42: NATURAL COURSE AND CLINICAL USEFULNESS. Front Biosci 7:d997–1006
32. Cselényi Z, Farde L (2015) Quantification of blood flow-dependent component in estimates of beta-amyloid load obtained using quasi-steady-state standardized uptake value ratio. J Cereb Blood Flow Metab 35(9):1485–1493
33. Ishii K, Yamada T, Hanaoka K, Kaida H, Miyazaki K, Ueda M et al (2020) Regional gray matter-dedicated SUVR with 3D-MRI detects positive amyloid deposits in equivocal amyloid PET images. Ann Nucl Med 34(11):856–863
34. Ashburner J (2007) A fast diffeomorphic image registration algorithm. NeuroImage 38(1):95–113
35. Ishii K (2002) Clinical application of positron emission tomography for diagnosis of dementia. Ann Nucl Med 16(8):515–525
36. Asada T, Kakuma T, Tanaka M, Araki W, Lebowitz AJ, Momose T et al (2025) A statistical method for predicting amyloid-β deposits from severity, extend, and ratio indices of the (99m)Tc-ECD SPECT. J Alzheimers Dis 104(4):1281–1289
37. Woyk K, Hansen N, Wiltfang J, Lange C, Bouter C (2025) The relationship of (18)F-FDG-PET to other common biomarkers of dementia in a clinical cohort with memory deficits. J Alzheimers Dis Rep 9:25424823251314392
38. Andriuta D, Moullart V, Schraen S, Devendeville A, Meyer ME, Godefroy O (2018) Inferior Parietal Cortex Hypoperfusion is the Most Specific Imaging Marker for AD Patients With Positive CSF Biomarker Assays in a Memory Clinic in France. Alzheimer Dis Assoc Disord 32(2):89–93
39. Habert MO, de Souza LC, Lamari F, Daragon N, Desarnaud S, Jardel C et al (2010) Brain perfusion SPECT correlates with CSF biomarkers in Alzheimer's disease. Eur J Nucl Med Mol Imaging 37(3):589–593
40. Tapiola T, Alafuzoff I, Herukka SK, Parkkinen L, Hartikainen P, Soininen H et al (2009) Cerebrospinal fluid {beta}-amyloid 42 and tau proteins as biomarkers of Alzheimer-type pathologic changes in the brain. Arch Neurol 66(3):382–389
41. Jagust WJ, Landau SM, Shaw LM, Trojanowski JQ, Koeppe RA, Reiman EM et al (2009) Relationships between biomarkers in aging and dementia. Neurology 73(15):1193–1199
42. Racine AM, Koscik RL, Nicholas CR, Clark LR, Okonkwo OC, Oh JM et al (2016) Cerebrospinal fluid ratios with Aβ42 predict preclinical brain β-amyloid accumulation. Alzheimers Dement (Amst) 2:27–38

43. Palmqvist S, Zetterberg H, Mattsson N, Johansson P, Minthon L, Blennow K et al (2015) Detailed comparison of amyloid PET and CSF biomarkers for identifying early Alzheimer disease. Neurology 85(14):1240–1249
44. Takayama T, Hirose T, Goto M, Daida H, Nakajima M, Nakanishi A et al (2026) Utility of Regional Cerebral Blood Flow SPECT and MRI for Predicting Amyloid Deposition in Real-World Clinical Settings. Psychogeriatrics 26(3):e70158
45. Bouter Y, Glasnek RM, Wenzel JM, Bouter C (2025) (18)F-FDG-PET and Multimodal Biomarker Integration: A Powerful Tool for Alzheimer's Disease Diagnosis. Nucl Med Mol Imaging 59(6):453–471
46. Bernetti C, D'Andrea V, Buoso A, Barbalace I, Greco F, Pilato F et al (2025) Arterial Spin Labeling MRI in Alzheimer's Disease: A Systematic Review of Cerebral Perfusion Biomarkers. J Neuroimaging 35(2):e70035
47. Tsougos I, Valotassiou V, Tsivaka D, Satra M, Angelidis G, Papatriantafyllou J et al (2026) SPECT and PET imaging of Alzheimer's disease revisited: from biomarkers to artificial intelligence-based prediction. Ann Nucl Med 40(5):480–495
48. Albert MS, DeKosky ST, Dickson D, Dubois B, Feldman HH, Fox NC et al (2011) The diagnosis of mild cognitive impairment due to Alzheimer's disease: recommendations from the National Institute on Aging-Alzheimer's Association workgroups on diagnostic guidelines for Alzheimer's disease. Alzheimers Dement 7(3):270–279
49. Matsuda H, Hanyu H, Kaneko C, Ogura M, Yamao T (2025) Highly specific amyloid and tau PET ligands for ATN classification in suspected Alzheimer's disease patients. Ann Nucl Med 39(5):458–465

Tables

Tables 1 to 6 are available in the Supplementary Files section.

Figures

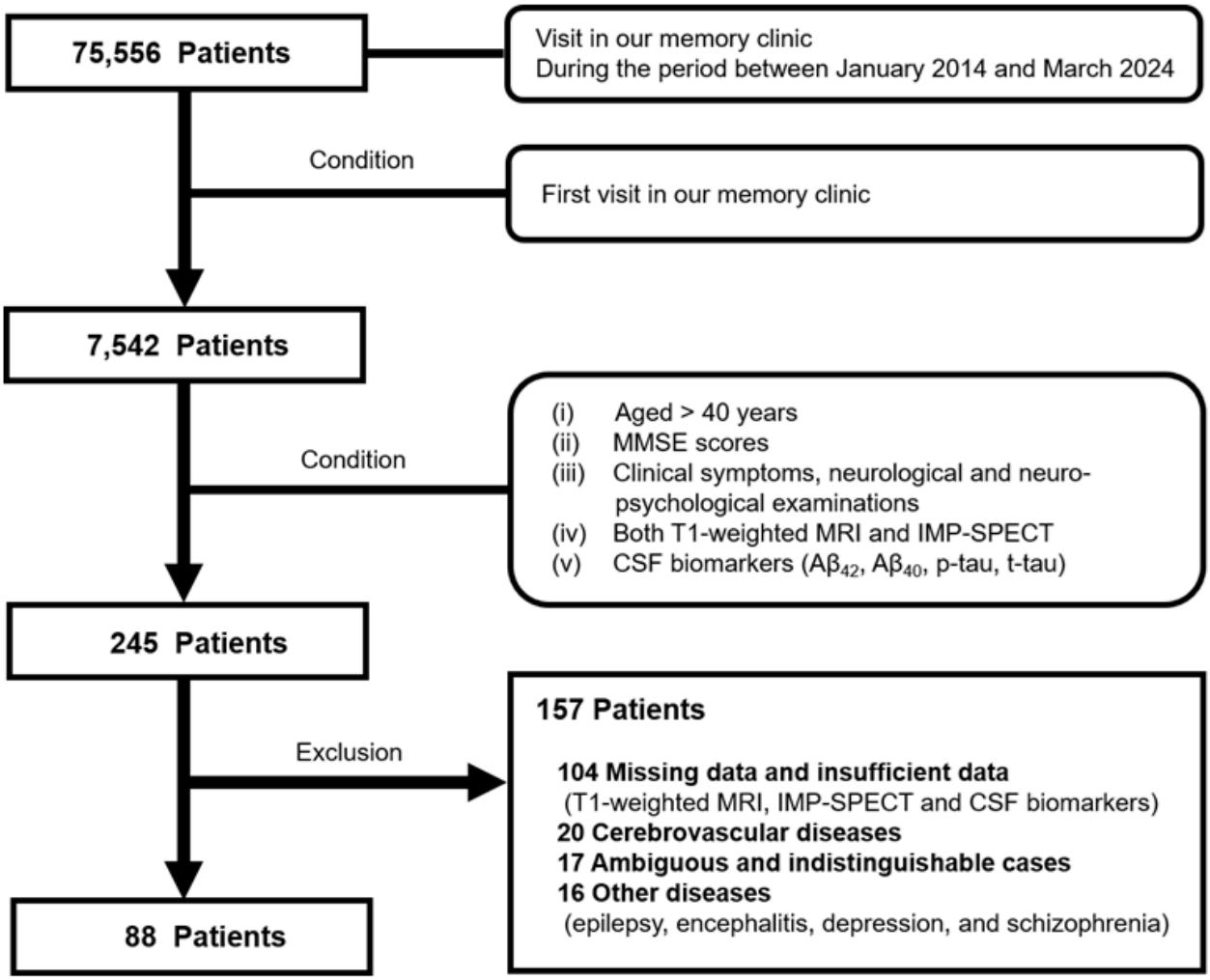


Figure 1

Flowchart of patient inclusion and exclusion

Over a period of 10 years, 7,542 patients first visited our memory clinic. Of these, 245 patients met our criteria in this study. After excluding 157 patients, 88 patients remained.

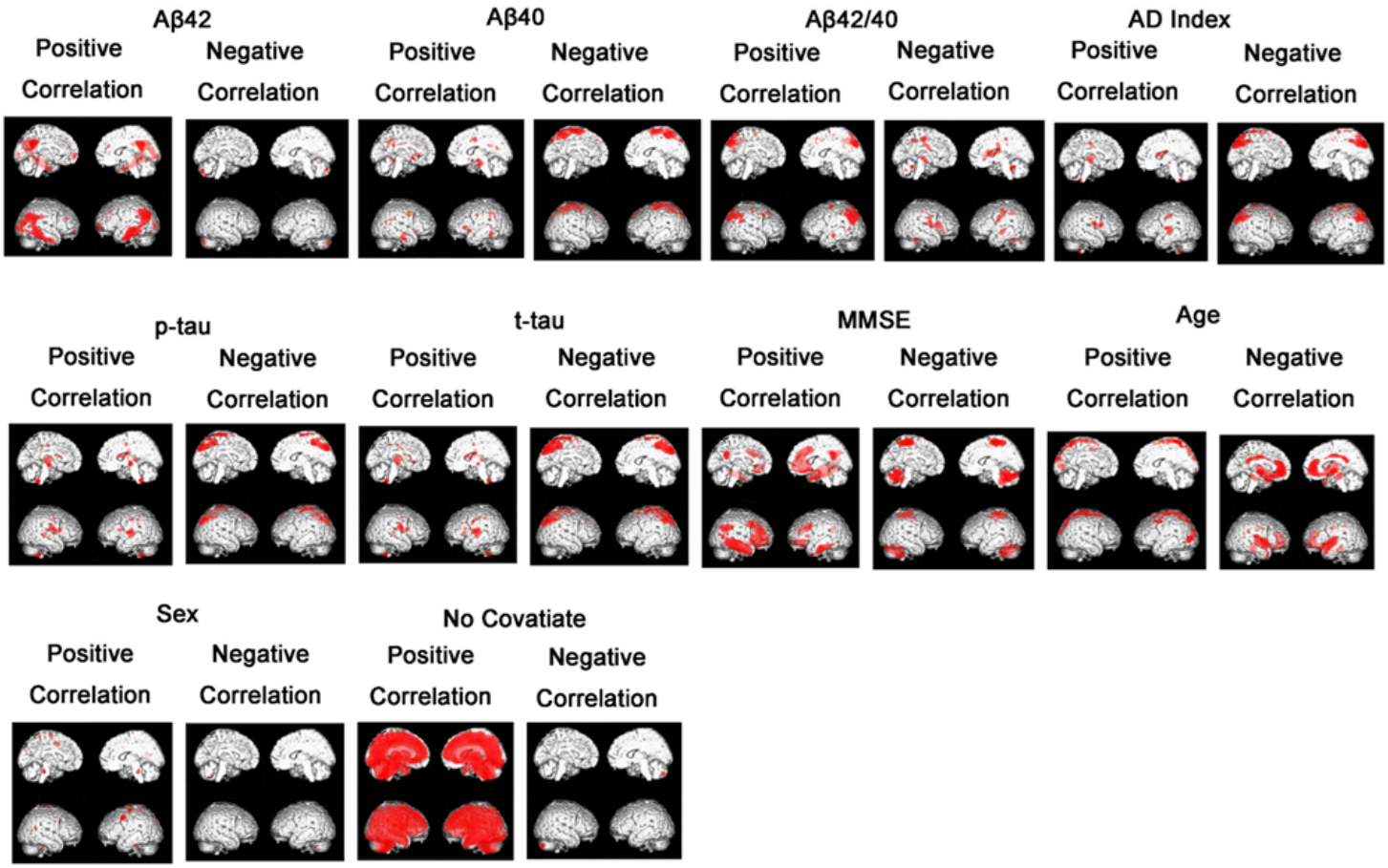


Figure 2

Hypoperfusion region with positive or negative correlations with CSF biomarkers, MMSE score, age and sex

Regions showing significant correlations are displayed in red.

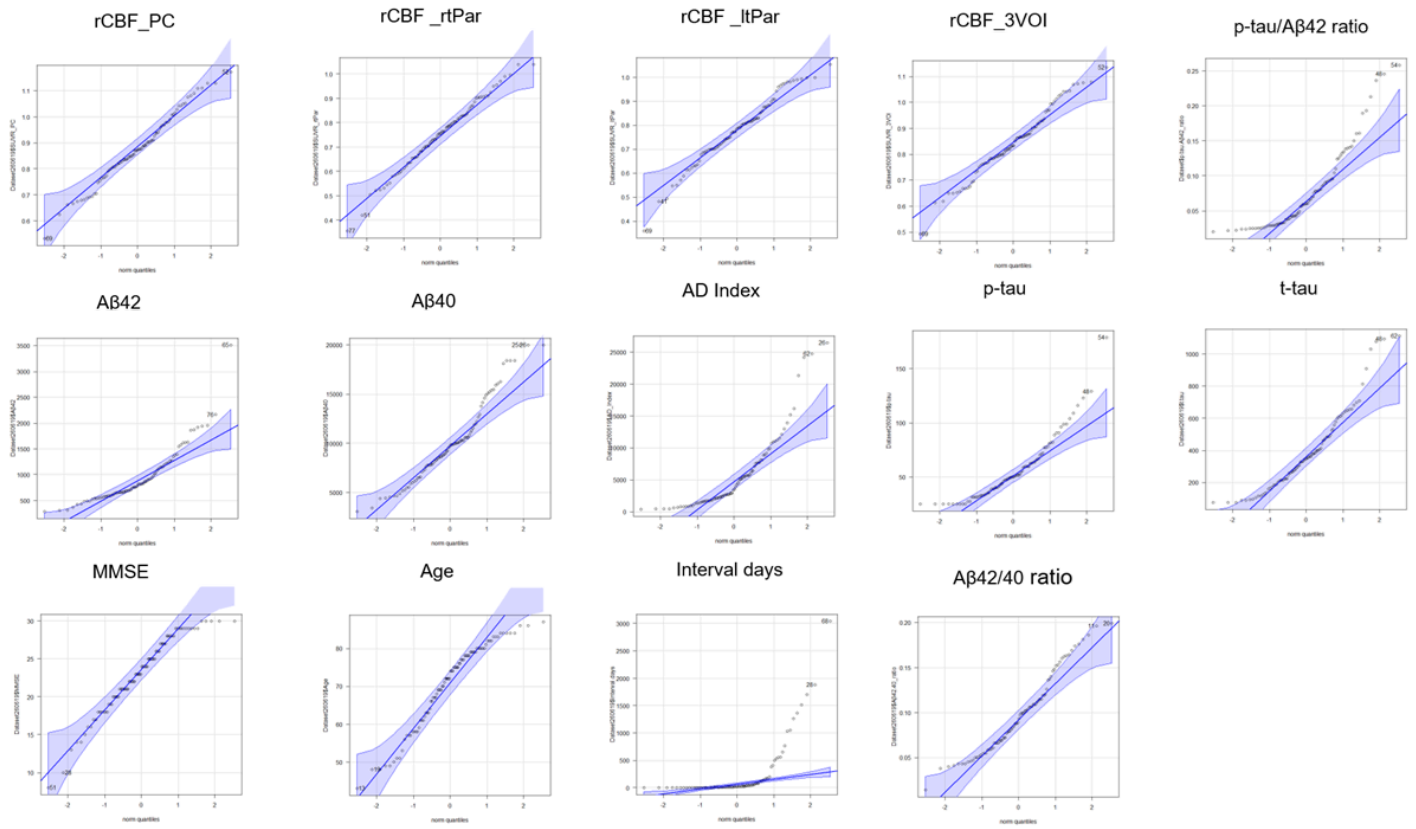


Figure 3

Quantile-Quantile plot (Q-Q plot)

Normality of data was evaluated using a normal Q-Q plot.

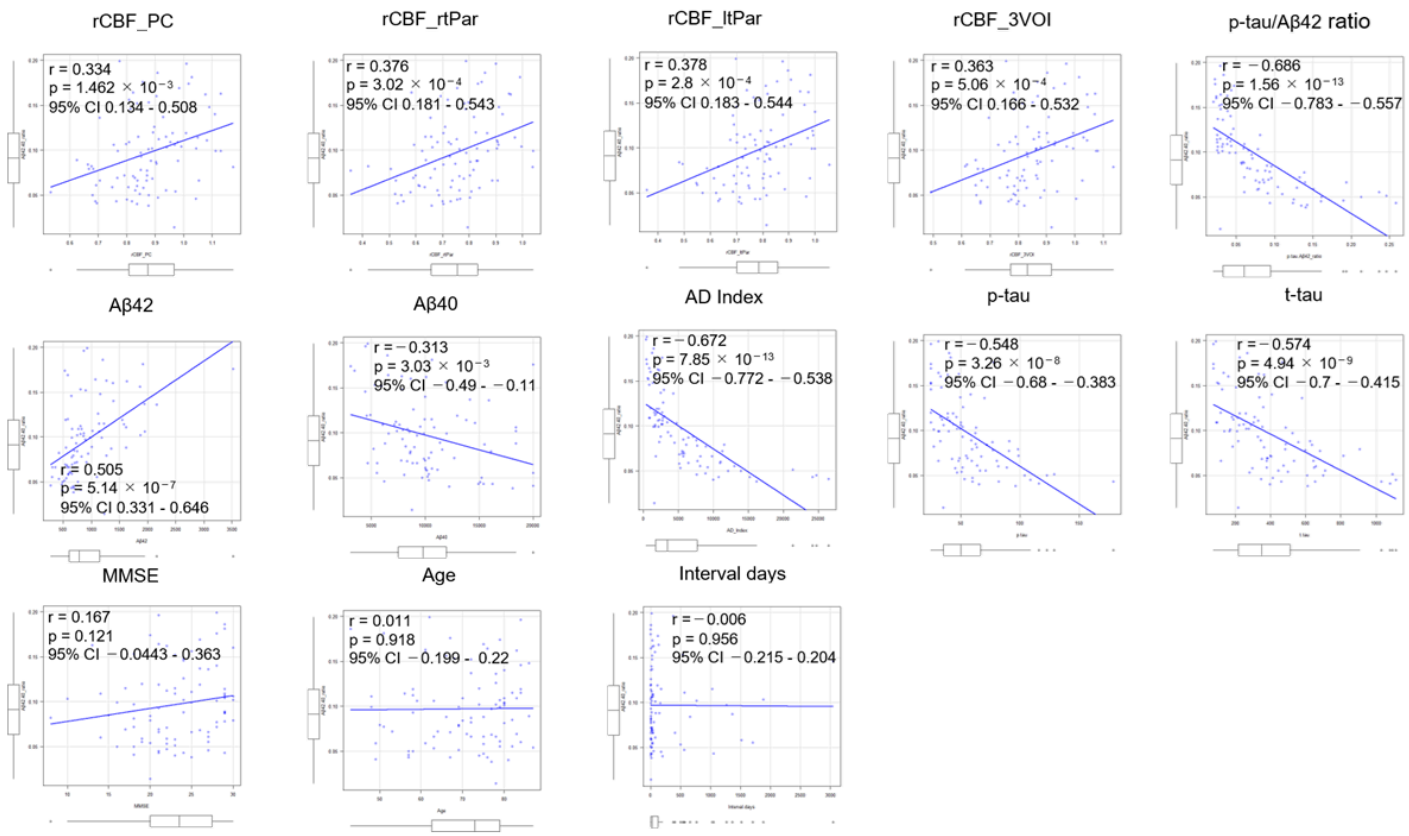


Figure 4

Correlation between CSF Aβ42/40 ratio and rCBF of each VOI

Pearson's correlation coefficient (PCC) between rCBF of each VOI and CSF Aβ42/40 ratio were presented, using various CSF biomarkers, MMSE, age and interval days as comparison.

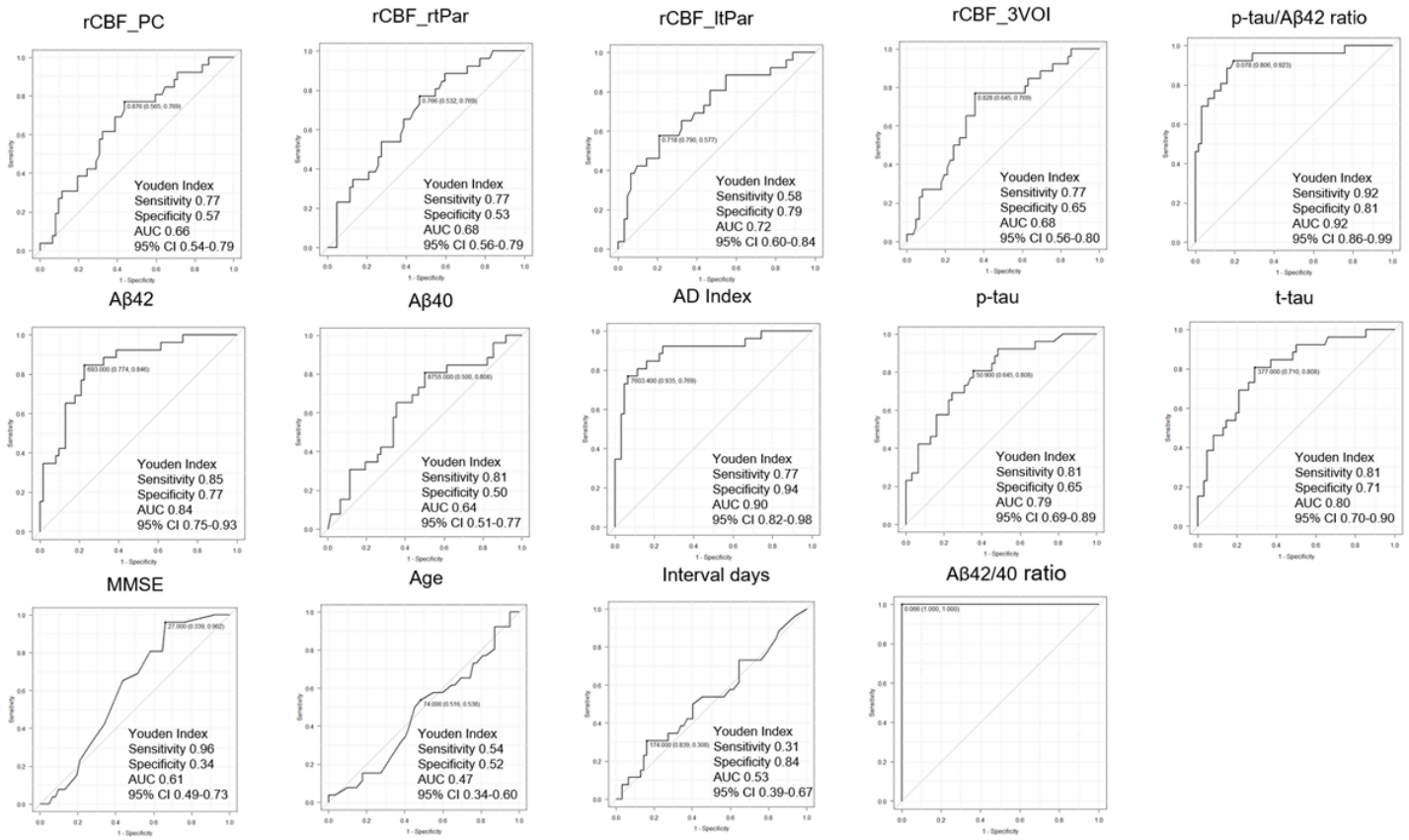


Figure 5

Estimation of Aβ deposition using rCBF of each VOI

CSF Aβ 42/40 ratio was set as the criterion for Aβ deposition in 88 patients. Correlation between Aβ deposition and rCBF of each VOI was compared with other CSF biomarker level, MMSE score, age, and interval days.

Supplementary Files

This is a list of supplementary files associated with this preprint. Click to download.

- Table1to6.docx